Pharmaceutical Research, Vol. 22, No. 2, February 2005 (© 2005)
DOI: 10.1007/s11095-004-1191-5

Research Paper

Pharmacokinetics of Substrate Uptake and Distribution in Murine Brain After Nasal Instillation

Candace L. Graff,[1] Rong Zhao,[1] and Gary M. Pollack[1,2]

Received September 8, 2004; accepted October 27, 2004

Purpose. This study was conducted to develop a physiologically relevant mathematical model for describing brain uptake and disposition of nasally administered substrates.
Methods. [^{14}C]-antipyrine, [^{14}C]-diazepam, [^{3}H]-sucrose, or [^{3}H]-verapamil was administered nasally to CF-1 mice. P-glycoprotein (P-gp)-deficient mice also received [^{3}H]-verapamil to probe the influence of P-gp on uptake/distribution. Mice were sacrificed at selected intervals, and 20 serial 300-μm coronal brain sections were obtained to determine radioactivity. A series of compartmental pharmacokinetic models was developed and fit to concentration vs. time/distance data.
Results. After nasal instillation, substrate concentration was highest in the olfactory bulb and decreased with distance. In the absence of transport-mediated flux, peak brain exposure occurred at 6 h. A catenary pharmacokinetic model with slice-specific brain-to-blood efflux rate constants and slice-to-slice diffusivity factors was capable of fitting the data. P-gp limited fractional absorption of [^{3}H]-verapamil via efflux from the nasal cavity and olfactory epithelium. P-gp also increased the rate constants associated with [^{3}H]-verapamil efflux 1.5- to 190-fold, depending on brain region. P-gp limited [^{3}H]-verapamil uptake from the nasal cavity into brain and facilitated removal of [^{3}H]-verapamil from brain during rostral-to-caudal distribution.
Conclusions. Taken together, the data and associated modeling provide a comprehensive assessment of the influence of P-gp on brain uptake and disposition of nasally administered substrates.

KEY WORDS: blood-brain barrier; brain slices; nasal administration; P-glycoprotein; pharmacokinetics.

INTRODUCTION

Treatment of central nervous system (CNS) disorders remains challenging, primarily due to the inability of potential therapeutic agents to reach the relevant pharmacologic target. The blood-brain barrier (BBB) forms a nearly impenetrable barrier that excludes compounds based on their physicochemical properties and affinity for active efflux transport (1). P-glycoprotein (P-gp) is a barrier transporter that limits brain uptake of substrates from a variety of therapeutic classes, including protease inhibitors, antiepileptics, and anticancer agents (2–4). P-gp is considered a prototypical multidrug resistance (MDR) transport protein, originally identified based on its ability to render cancer cells resistant to chemotherapy (5), and is the most well characterized of the BBB efflux transport systems. P-gp is a 170-kDa plasma membrane, energy-dependent efflux protein that is a member of the ABC superfamily of transport systems (6,7) and is expressed on the luminal side of the brain capillary endothelium (8). P-gp expels a wide range of functionality and structurally unrelated compounds from the endothelial cell. In general, P-gp substrates are hydrophobic, amphipathic molecules with a planar ring system, a molecular weight >400 kDa, and a positive charge at pH 7.4 (9). However, due to the complexities involved with multiple substrate and ATP binding sites and conformational changes secondary to substrate binding, no comprehensive structure-activity relationships have been established for P-gp (10).

Due to the formidable obstacle imposed by the BBB, there has been increased interest in developing strategies to overcome this barrier. It has been a widely held view that nasal delivery provides a means to circumvent the BBB and thus may allow increased CNS penetration of compounds that otherwise display limited CNS exposure (11). In general, there are three pathways that a drug administered into the nasal cavity may travel. These routes include entry into the systemic circulation directly from the nasal mucosa (12), entry into the olfactory bulb via axonal transport along neurons (13), and direct entry into the brain via the olfactory epithelium (14). A drug that enters into the systemic circulation must be absorbed through the nasal mucosa. Administration via this route avoids hepatic/GI first-pass effects and therefore may provide more extensive systemic exposure for substrates that have poor oral bioavailability (15). However, this particular route does not represent an advantage for the delivery of agents to the CNS (as the substrate must traverse the BBB from the systemic circulation), and is thus not a focus of this paper. A drug also may be carried along the olfactory

[1] Division of Drug Delivery and Disposition, School of Pharmacy, University of North Carolina, Chapel Hill, North Carolina 27599, USA.
[2] To whom correspondence should be addressed. (e-mail: gary_pollack@unc.edu)

neuron by intracellular axonal transport to the olfactory bulb. This olfactory nerve pathway would allow the drug to be taken up into the neuronal cell (located in the olfactory epithelium) by endocytosis and subsequently transported into the CNS. This pathway is used by some metals, viruses, and proteins (13,16,17) and represents a path by which the BBB may be bypassed. Despite the ability of this pathway to deliver agents to the olfactory bulb, transport to CNS sites beyond the olfactory system is unclear. Furthermore, this route is slow (requiring hours to days to reach certain brain regions), and thus cannot account for the immediate appearance (within minutes) of some solutes in the brain and/or CSF after nasal administration. The mechanisms governing direct delivery of substrate to the brain via the olfactory epithelium are not well understood. This pathway purportedly involves delivery of the substrate directly to the brain parenchymal tissue, to the cerebrospinal fluid (CSF), or to both (18). Although the BBB does not exist at the olfactory epithelium, P-gp (and likely other BBB transporters) is functional at this barrier (19). The experiments reported in this communication were designed to explore the kinetics of brain uptake and distribution via this direct olfactory epithelial pathway.

There is increasing evidence that a direct nose-to-brain pathway (resulting in rapid brain uptake) exists and can be accessed by a variety of compounds in both rodent models and humans (14,20,21). To exploit this direct olfactory epithelial route of delivery, a compound must cross the olfactory membrane via the transcellular pathway or via the paracellular pathway. The former route is used by small lipophilic (primarily by diffusion) or large molecules (primarily by receptor-mediated endocytosis), while the latter route is used by small hydrophilic molecules (22). There are a variety of factors that will affect the permeability of nasally delivered drugs, including the biology of the system (i.e., structural features, pH, mucociliary clearance, and biochemical factors such as enzymes) and formulation factors [i.e., physicochemical properties of the drug and formulation (23)]. For instance, it has been shown that the uptake of drugs into the CSF and brain parenchyma is dependent on molecular weight and lipophilicity. It is clear that a comprehensive understanding of the mechanisms governing this pathway is necessary in order to investigate the use of nasal administration as a practical means of delivering agents to the brain.

Many of the studies examining brain uptake after nasal administration have used CSF concentrations as a surrogate for brain exposure. This may not be an accurate representation of pharmacologically relevant CNS penetration since CSF is not necessarily in equilibrium with brain tissue. Other experimental protocols have determined substrate in whole brain, which provides an estimate of overall brain exposure but gives no information regarding localization within the brain. Although regional exposure has been addressed with microdialysis, this method provides information for only one discrete location per animal. Previous studies in this laboratory used whole brain homogenate (24), and thus the potential distribution of substrate within the brain, and the pharmacologic implications associated with this distribution, were unclear (19). Therefore, the purpose of the current study was to examine the kinetics of rostral-to-caudal distribution of nasally administered compounds (in the absence of transporter-mediated flux) and to develop a mathematical model to explain the disposition of these model compounds. In addition, the impact of P-gp–mediated efflux on brain uptake and distribution was considered with the standard P-gp substrate verapamil.

MATERIALS AND METHODS

Materials

Probe substrates were obtained from the following sources: [^{3}H]-(±)-verapamil (85 Ci/mmol), [^{14}C]-diazepam (56 mCi/mmol), and [^{3}H]-sucrose (10.2 Ci/mmol) from NEN Life Science Products (Boston, MA, USA); [^{14}C]-antipyrine (55 mCi/mmol) from American Radiolabeled Chemicals (St. Louis, MO, USA). All other reagents used in this study were of the highest grade available from commercial sources.

Animals

Adult CF-1 mice [*mdr1a*(+/+) and *mdr1a*(–/–), 30–40 g, 8–12 weeks of age] were purchased from Charles River Laboratories (Wilmington, MA, USA) and maintained in a breeding colony in the School of Pharmacy, The University of North Carolina. Male and female mice were housed separately (maximum of 4 animals per cage) in wire-mesh cages in a temperature- and humidity-controlled room with a 12-h dark/12-h light cycle and had unrestricted access to food and water. The Institutional Animal Care and Use Committee of the University of North Carolina approved the experimental protocols, and all procedures were conducted according to the Principles of Laboratory Animal Care (NIH Publication No. 85-23, revised 1985).

Nasal Administration

Nasal administration was performed as previously reported (19). Briefly, mice (n = 4/group) were anesthetized by intraperitoneal injection of ketamine and xylazine (140 and 8 mg/kg, respectively). The mice were placed in a supine position on a 37°C heating pad to maintain body temperature with the head held back and a dowel (~7 mm) under the neck to limit liquid flow down the trachea. Solutions containing test compounds (pH 7) were warmed to 37°C in a water bath prior to instillation. Tracers were added at a concentration of 0.5 mCi/ml. The solutions (5 μM, 5 μl/nostril) were administered via separate 10-μl gas-tight syringes (2-inch, 23-gauge needle) to each nostril. Timing for the purpose of determining substrate uptake was initiated after completion of instillation. The animals were allowed free mobility upon awakening from the anesthesia. Brain uptake was terminated by decapitation at pre-determined time points (2, 4, 6, 8, 10, 12, 18 h post-dose). The brain was removed rapidly from the skull, blotted dry, and mounted on a platform with cyanoacrylate to allow coronal slicing.

Systemic Administration

Mice (n = 4/group) were anesthetized as described above. Substrates (5 mg/kg in 50% methanol) with appropriate tracers (0.5 mCi/ml) were administered via tail vein injection (<0.01 ml/g). Brain uptake was terminated by decapitation at 2, 6, or 10 h post-dose. After the experiment, the brain was removed and prepared for slicing as described above.

Fresh Tissue Slicing

After allowing the tissue to set for approximately 2 min, the platform was submersed in 2°C phosphate buffered saline (PBS) for slicing (Vibratome 3000, St. Louis, MO, USA). Coronal sections (300 μm) were cut with a 35°-blade angle using Vibratome feather blades [low speed (setting 1), high amplitude (setting 8)]. Sequential slices were obtained in the rostral to caudal direction. Slices were removed from the buffer and placed in tared 8-ml glass scintillation vials and weighed. The tissue was digested with 0.3 ml Solvable (Packard, Boston, MA, USA) at 50°C overnight. After cooling, samples were mixed with 5 ml scintillation cocktail (Ultimate Gold XR; Packard) and total radioactivity was determined. Scintillation counting (referenced to appropriate quench curves for single- or dual-label counting, depending on the experiment) was performed in a Packard Tri-Carb model 1900 TR (Packard). Brain samples obtained from naïve mice were analyzed, and these blanks were subtracted from all samples to correct for apparent background.

Data Analysis

Data are expressed as mean ± SD (n = 4) unless otherwise noted. Where appropriate, a two-tailed Student's *t* test was used to evaluate the statistical significance of differences between experimental groups. In all cases, $p < 0.05$ was used as the criterion of statistical significance.

The total fraction of radioactivity in the whole brain at each time point was calculated as the percentage of the total amount of radioactivity in the administered dose:

$$\text{Fraction}\,(\%) = \frac{\text{Amount (dpm/mg, brain)} * \text{brain weight (mg)}}{\text{Total dose administered (dpm)}} \times 100$$

The area under the slice concentration-time curve ($AUC_{0\rightarrow18}$ for nasal administration, $AUC_{0\rightarrow10}$ for systemic administration) was calculated to assess the regional exposure from time zero to 18 h after nasal administration (and time zero to 10 h after systemic administration) according to the linear trapezoidal method.

Pharmacokinetic Modeling

Mean data for substrate concentration in each slice at each time point were fit simultaneously with the scheme depicted in Fig. 1A. Because the substrate dose used in these experiments was low, linear conditions were assumed. The model incorporated first-order absorption from the nasal cavity into brain (k_a), with subsequent passive diffusion in the rostral-to-caudal direction between adjacent slices (k_{12}). It was assumed that the slice-to-slice diffusion rate constant was independent of brain region. Flux from the nasal cavity (k_n), as well as from each individual slice (k_{oi}) was included. To account for the different physicochemical properties of the substrates (i.e., lipophilicity), diffusivity factors (Df_j for each compound *j*) were used as a modulator of the absorption rate constant (k_a) and the rate constant for slice-to-slice diffusion (k_{12}).

The amount of [^{14}C]-diazepam or [^{14}C]-antipyrine in wild-type mice, and [^{3}H]-verapamil in *mdr1a*(–/–) animals, in each brain slice was modeled vs. time with the following differential equations:

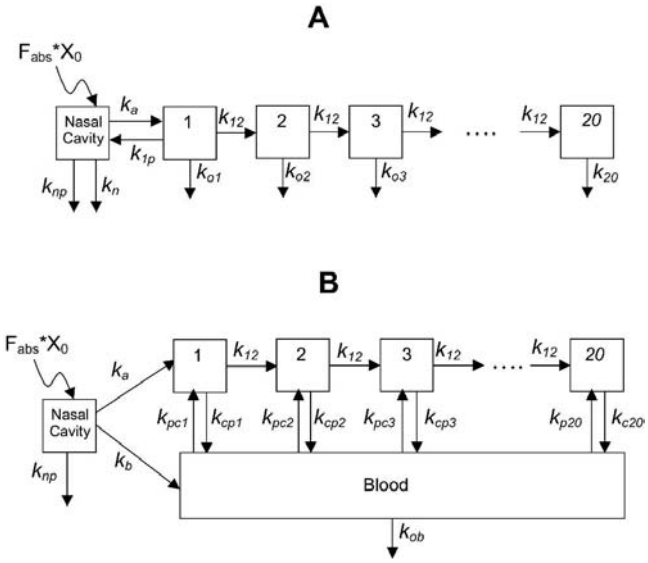

Fig. 1. (A) Scheme of the model for brain uptake and disposition after nasal administration via the olfactory epithelium. F_{abs} represents the fraction of dose absorbed with X_0 representing the dose. k_a represents the apparent first-order absorption rate constants into brain from the nasal cavity; k_n represents the first-order rate constant for non-P-gp–mediated flux from the nasal cavity; k_{1p} and k_{np} are first-order rate constants representing P-gp–mediated flux from the brain and nasal cavity, respectively; k_{12} represents the first-order rate constant for passive diffusion between adjacent slice compartments (in a rostral-to-caudal direction only); and k_{oi} represents the first-order rate constant for the passive diffusion out of the *i*th brain section. Diffusivity factors were included in the final model structure to account for the lipophilicy of each compound and were incorporated into k_a and k_{12}. (B) Scheme of the best model fit for brain uptake via systemic circulation after nasal administration. The parameters are the same as for model A with additional parameters representing absorption into blood (k_b), absorption rate constants for flux between blood and brain (k_{pci} and k_{cpi}), and flux out of blood (k_{ob}).

In the nasal cavity,

$$\frac{dX_{\text{nasal}}}{dt} = -(Df_j \cdot k_a \cdot X_{\text{nasal}}) - (k_n \cdot X_{\text{nasal}})$$

For the first slice,

$$\frac{dX_1}{dt} = (Df_j \cdot k_a \cdot X_{\text{nasal}}) - (Df_j \cdot k_{12} \cdot X_1) - (k_{o1} \cdot X_1)$$

For all subsequent slices,

$$\frac{dX_i}{dt} = (Df_j \cdot k_{12} \cdot X_{(i-1)}) - (k_{oi} \cdot X_i) - (Df_j \cdot k_{12} \cdot X_i)$$

For the last slice,

$$\frac{dX_{20}}{dt} = (Df_j \cdot k_{12} \cdot X_{19}) - (k_{o20} \cdot X_{20})$$

where at $t = 0$, $X_{\text{nasal}} = F_{\text{abs}}{}^{*}X_0$ (X_0 was the dose administered); for all subsequent slices, the initial value X_i ($i = 2\rightarrow20$) was equal to zero at time zero.

To account for the impact of P-gp on [^{3}H]-verapamil disposition, additional flux parameters were incorporated from the brain (k_{1p}) and the nasal cavity (k_{np}). In order to

determine the value of k_{np}, k_n was fixed at 1.87 h^{-1}, the value determined in the absence of P-gp–mediated efflux (i.e., from [^{3}H]-verapamil disposition in *mdr1a*(–/–) mice).

The amount of [^{3}H]-verapamil in each brain slice of *mdr1a*(+/+) animals was modeled vs. time with the following differential equations:

In the nasal cavity,

$$\frac{dX_{\text{nasal}}}{dt} = -[(k_{np} + k_n) \cdot X_{\text{nasal}}] - (Df_j \cdot k_a \cdot X_{\text{nasal}}) + (k_{1p} \cdot X_1)$$

For the first slice,

$$\frac{dX_1}{dt} = (Df_j \cdot k_a \cdot X_{\text{nasasl}}) - (k_{1p} \cdot X_1) - (k_{o1} \cdot X_1) - (Df_j \cdot k_{12} \cdot X_1)$$

For all subsequent slices,

$$\frac{dX_i}{dt} = (Df_j \cdot k_{12} \cdot X_{(i-1)}) - (k_{oi} \cdot X_i) - (Df_j \cdot k_{12} \cdot X_i)$$

For the last slice,

$$\frac{dX_{20}}{dt} = (Df_j \cdot k_{12} \cdot X_{19}) - (k_{o20} \cdot X_{20})$$

where the initial conditions for each slice were as defined above for *mdr1a*(–/–) animals.

A model based on the scheme depicted in Fig. 1B was used to determine whether systemic concentrations contributed significantly to the brain uptake and disposition of model substrates. This model was similar to model A but incorporated a first-order absorption into blood from the nasal cavity (k_b) and bidirectional flux from blood into the sequential slices (k_{pci}, k_{cpi}). It also allowed for elimination of substrate from the blood compartment (k_{ob}).

Model differential equations were fit to the mean data by nonlinear least-squares regression with WinNonlin software (Pharsight, Palo Alto, CA, USA). Assessment of the goodness of fit of the model to the observed data was based on coefficients of variation (CV%) and distribution of residual error. Akaike's Information Criteria (AIC) was used to compare the appropriateness of alternative model structures.

RESULTS

Brain Uptake After Nasal Instillation

For all of the compounds studied, the total amount present in the brain (expressed as % dose) after nasal instillation peaked at 6 h post-dose (Fig. 2). [^{14}C]-diazepam had the highest amount in brain at 6 h (3.58 ± 0.28%), followed by [^{3}H]-verapamil in the *mdr1a*(–/–) mice (3.16 ± 0.74%) and [^{14}C]-antipyrine (2.84 ± 0.34%). In general, the temporal profiles of these compounds were similar. In contrast, [^{3}H]-sucrose showed very limited uptake (0.91 ± 0.22%), and although the amount in brain peaked at 6 h, the profile evidenced little relationship with time. The *mdr1a*(+/+) mice exhibited much lower brain uptake of [^{3}H]-verapamil compared to *mdr1a*(–/–) animals (1.2 ± 0.31% at 6 h; $p < 0.001$), consistent with P-gp–mediated efflux. The total amount delivered to the brain (expressed as $AUC_{0\rightarrow18}$) varied among the substrates examined, with [^{14}C]-diazepam displaying the highest exposure (32.8 ± 6.3 %dose*h/mg), followed by [^{3}H]-verapamil in the *mdr1a*(–/–) mice (29.5 ± 5.3 %dose*h/mg) and [^{14}C]-antipyrine (26.2 ± 4.8 %dose*h/mg). [^{3}H]-sucrose and [^{3}H]-verapamil in the *mdr1a*(+/+) mice both displayed markedly lower brain exposure (8.3 ± 2.3 and 10.2 ± 2.1 %dose*h/mg, respectively; $p < 0.01$ for [^{3}H]-verapamil compared to *mdr1a*(–/–) animals). In the absence of an influence of P-gp, the amount delivered to the brain correlated significantly ($r^2 = 0.95$) with the log p values of the model substrates (Fig. 3).

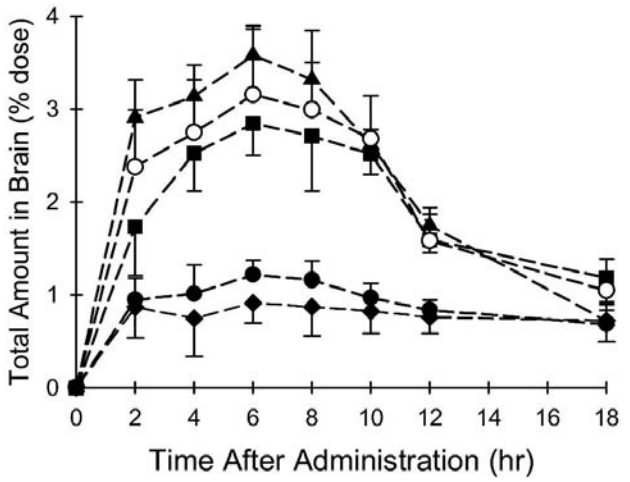

Fig. 2. Time course of [^{14}C]-diazepam (triangles), [^{14}C]-antipyrine (squares), [^{3}H]-sucrose (diamonds), and [^{3}H]-verapamil [circles, closed in *mdr1a*(+/+), open in *mdr1a*(–/–) animals] after nasal administration represented as %dose in brain. Symbols represent mean ± SD (n = 4).

Brain Distribution After Nasal Instillation

Regional exposure (i.e., exposure in each brain tissue slice; dose-normalized and expressed as $AUC_{0\rightarrow18}$) differed among the model substrates (Fig. 4). As was the case with total brain content, [^{14}C]-diazepam exhibited the highest exposure in each slice, followed by [^{3}H]-verapamil in *mdr1a*(–/–) animals, [^{14}C]-antipyrine, [^{3}H]-sucrose and [^{3}H]-verapamil in *mdr1a*(+/+) animals. Exposure was highest in the olfactory region (slices nos. 1–3) and decreased toward the more rostral

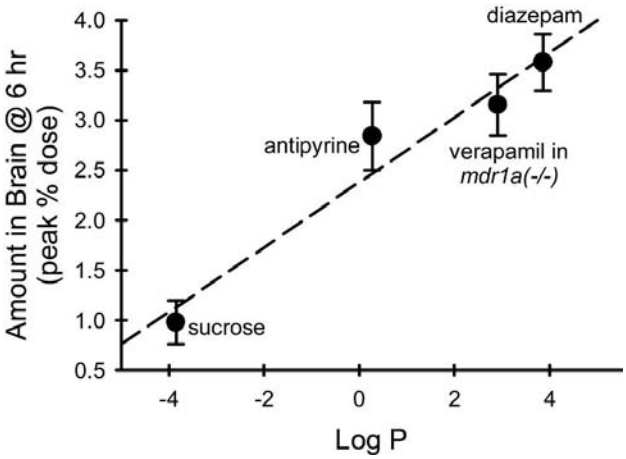

Fig. 3. Relationship between the peak amount of drug delivered to the brain after nasal administration and reported log p values. Data represent mean ± SD (n = 4), and the line represents the linear regression through those points ($r^2 = 0.95$).

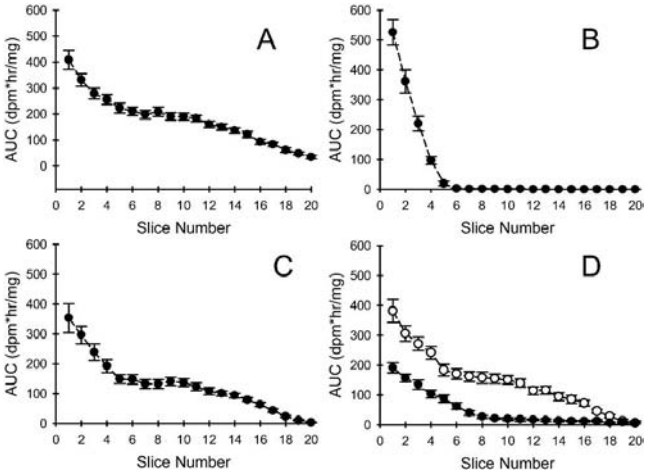

Fig. 4. Regional exposure (expressed as $AUC_{0\rightarrow18}$) resulting from the distribution of substrates after nasal administration. Symbols represent mean ± SD (n = 4). Panel A describes the distribution of [^{14}C]-diazepam, panel B describes the distribution of [^{3}H]-sucrose, panel C describes the distribution of [^{14}C]-antipyrine, and panel D describes the distribution of [^{3}H]-verapamil [● in *mdr1a*(+/+) and ○ in *mdr1a*(–/–) animals].

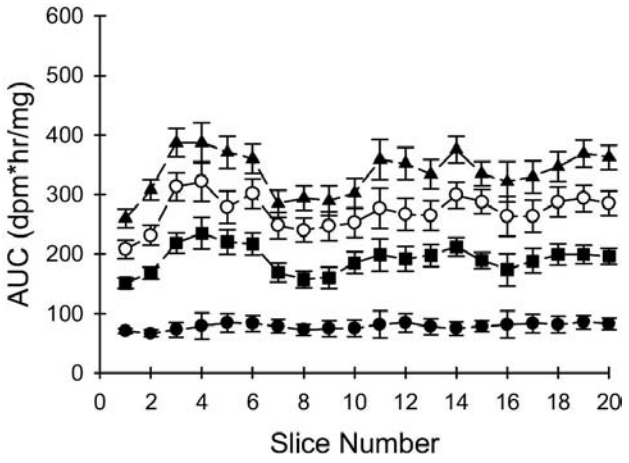

Fig. 5. Regional exposure of substrates (expressed as $AUC_{0\rightarrow10}$) after systemic administration. Triangles represent [^{14}C]-diazepam, squares represent [^{14}C]-antipyrine, and circles represent [^{3}H]-verapamil [open in *mdr1a*(–/–) and closed in *mdr1a*(+/+) animals]. Data are mean ± SD (n = 4 per group).

portions of the brain. In addition, [^{3}H]-sucrose evidenced virtually no substrate exposure beyond slice no. 5.

Brain Uptake and Distribution After Systemic Administration

To assess the difference in brain distribution after nasal administration compared to systemic administration, the model compounds also were administered systemically (i.v.) to mice, and both total amount delivered (% dose) and total exposure ($AUC_{0\rightarrow10}$) were determined. Systemic administration resulted in a larger fraction of the dose being delivered to the brain for each of the compounds, and the peak amount in brain occurred at 2 h (compared to 6 h for nasal administration). The peak brain content was 11.7 ± 2.6, 8.7 ± 2.3, 5.9 ± 1.8, and 1.3 ± 0.4% for [^{14}C]-diazepam, [^{3}H]-verapamil in *mdr1a*(–/–) mice, [^{14}C]-antipyrine and [^{3}H]-verapamil in *mdr1a*(+/+) mice, respectively. There was no [^{3}H]-sucrose detectable in the brain after systemic administration.

The regional exposure also differed between systemic administration compared to nasal administration (Fig. 5). Substrate content after systemic administration was relatively constant across the slices; certainly, preferential accumulation in specific slices was not evident. However, the amount of substrate in slices nos. 7–10 was lower than in other areas of the brain. These slices correspond anatomically with regions containing the striatum, parietal cortex and thalamus, structures that have relatively low blood volumes (25).

Pharmacokinetic Modeling

Serial coronal tissue slicing was used in the current investigation to examine the distribution of substrates in the brain. The primary objective of this study was to determine the effect of lipophilicity and P-gp–mediated efflux on substrate uptake into and distribution within the brain. Thus, a compartmental modeling approach was selected to analyze the data comprehensively. A model based on the scheme depicted in Fig. 1A was fit simultaneously to the substrate concentration vs. slice and time data. Representative descriptions of the data for individual slices are shown in Fig. 6. These panels illustrate the difference in [^{3}H]-verapamil distribution between P-gp–competent and P-gp–deficient mice. Final parameter estimates describing the brain distribution of substrates after nasal instillation in the presence and absence of P-gp are shown in Table I. In the presence as compared to absence of P-gp, the efflux rate constants for [^{3}H]-verapamil in each individual slice increased (1.4- to 190-fold, depending on brain region), indicative of increased efflux mediated by P-gp within the brain. The presence of P-gp also necessitated the inclusion of two additional flux components, one from the nasal cavity (k_{np}) and one at the olfactory epithelium (k_{1p}). These localizations are supported anatomically, given that P-gp has been identified in the nasal mucosa (26) and work in this laboratory has demonstrated the presence of P-gp in the olfactory epithelium (unpublished data). The P-gp–mediated efflux from the nasal cavity was larger than at the olfactory epithelium (8.92 vs. 4.32 h^{-1}, respectively), consistent with the larger surface area of the nasal cavity compared to the olfactory epithelium. The absorption of substrate (from nasal cavity to brain, k_a) was decreased in the presence of P-gp (0.126 vs. 0.0835 h^{-1}), consistent with P-gp–mediated efflux at this barrier resulting in a reduced rate of absorption. The slice-to-slice diffusional component of the model (k_{12}) remained essentially the same regardless of the presence of P-gp, indicating that the difference in disposition was due primarily to the transporter mediating egress from the brain. It is interesting to note that the diffusivity factors recovered correlated quite well with the reported log p values (and peak % dose absorbed) of these compounds (r^2 = 0.98).

Three-dimensional representations (comparing amount of substrate vs. time vs. slice number) of the model fit for the distribution of [^{14}C]-diazepam, [^{14}C]-antipyrine and [^{3}H]-verapamil (in *mdr1a*(–/–) and *mdr1a*(+/+) mice) are shown in Figs. 7–10, respectively. These profiles clearly demonstrate that substrate exposure is dependent on time after administration, slice number (i.e., specific brain region), lipophilicity (by comparing different substrates), and transporter specific-

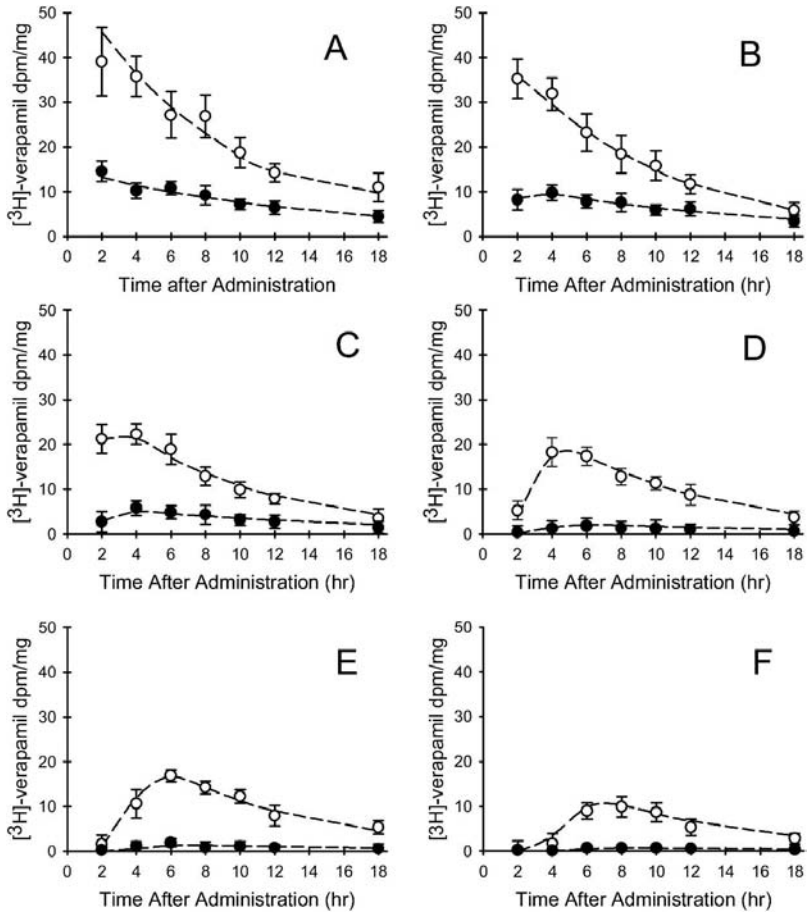

Fig. 6. Representative fit of the model to data from individual brain slices after nasal administration. Data are mean ± SD (n = 4); the line indicates the model fit. Open symbols indicate [^{3}H]-verapamil in *mdr1a*(–/–) animals and closed circles indicate [^{3}H]-verapamil in *mdr1a*(+/+) animals. The individual slices shown are slice no. 1 (A), slice no. 3 (B), slice no. 5 (C), slice no. 9 (D), slice no. 11 (E), and slice no. 14 (F). These slices were selected as representative of different brain regions and illustrate typical goodness-of-fit of the model to the data.

ity. In addition, each of these profiles evidenced a consistent plateau in slices obtained from the mid-brain.

To consider the impact of P-gp beyond the olfactory epithelium, the [^{3}H]-verapamil efflux parameters for individual slices in the presence vs. the absence of P-gp were compared, yielding slice-specific P-gp effects (Fig. 1I). The influence of P-gp on [^{3}H]-verapamil efflux from brain was dependent on brain region, with the highest P-gp effects observed in slices nos. 6–10. Alternative models that included various combinations of rate constants and altered compartmental structure were evaluated. For instance, the addition of a blood compartment for only slices nos. 1–3 (corresponding to the olfactory region) was included with bidirectional flux to account for multiple routes of substrate input at this site (from nasal cavity and the systemic circulation). In order to assess the potential for brain uptake occurring via the systemic circulation (after rapid absorption through the nasal mucosa), the model structure shown in Fig. 1B was considered. The data did not support these alternative models, as evidenced by a poor distribution of residual error, increased coefficients of variation for model parameters, and increased AIC. In addition, adjacent slices with similar substrate concentrations and common anatomic structures were grouped and included as lumped compartments. Bidirectional passive diffusion between adjacent slices also was considered, as were various feedback loops. Ultimately, the model structure and data analysis approach (Fig. 1A) chosen were superior and provided the best description of the observed data.

DISCUSSION

The compounds selected for this study were chosen based on physicochemical properties (lipophilicity, molecular weight) and to probe the influence of P-gp on brain uptake from the nasal cavity and subsequent distribution in the organ. Sucrose was selected to assess the feasibility of utilizing the nasal route to deliver a bulky hydrophilic compound that is unable to cross the BBB. Diazepam was chosen as a highly lipophilic model compound, the brain uptake of which has been shown to be blood flow–limited (25). Antipyrine was included in the compound set due to its intermediate lipophilicity. Finally, verapamil was chosen as a model P-gp substrate to study the effects of P-gp–mediated efflux on brain uptake and distribution.

In the absence of transporter-mediated flux ([^{3}H]-verapamil in *mdr1a*(–/–) mice; all other compounds in wild-type animals), the peak fraction of the dose in brain correlated well with the log p values for this compound set (Fig. 3). This observation suggests that brain uptake from the nasal cavity was mediated by the direct olfactory route and is con-

Table I. Final Model Parameters Associated with the Brain Distribution of [^{3}H]-Verapamil After Nasal Instillation

Parameter (h^{-1})	Parameters in the absence of P-gp		Parameters in the presence of P-gp		Parameter ratio
	Estimate	CV%	Estimate	CV%	
k_a	0.126	6.82	0.0835	24.8	0.663
k_{12}	1.32	10.8	1.19	43.5	0.902
k_{o1}	5.48	129	7.62	113.8	1.39
k_{o2}	1.21	46.9	3.22	78.5	2.66
k_{o3}	0.496	47.7	1.75	62.3	3.53
k_{o4}	0.584	47.0	1.23	48.8	2.11
k_{o5}	0.610	56.2	1.12	32.5	1.84
k_{o6}	0.151	78.9	0.872	78.2	5.77
k_{o7}	0.216	62.3	3.27	48.2	15.14
k_{o8}	0.0204	212	2.24	198.8	110
k_{o9}	0.0110	168	2.11	223.6	192
k_{o10}	0.0831	150	2.87	143.4	34.5
k_{o11}	0.319	78.3	0.983	87.2	3.08
k_{o12}	0.521	59.3	1.23	56.8	2.36
k_{o13}	0.186	61.2	0.822	48.8	4.42
k_{o14}	0.394	78.2	1.29	112.5	3.27
k_{o15}	0.451	34.6	1.89	89.8	4.19
k_{o16}	0.649	48.8	1.24	65.7	1.91
k_{o17}	0.893	52.1	2.74	49.9	3.07
k_{o18}	1.27	57.3	3.21	123.4	2.53
k_{o19}	1.89	47.5	3.78	65.4	2.00
k_{o20}	4.89	68.9	7.13	43.4	1.46
k_n	1.87	168	1.87	187.7	1
k_{np}	n/a	—	8.92	72.3	n/a
k_{1p}	n/a	—	4.32	68.2	n/a
F_{abs} (%)	2.03	78.5	2.03	84.8	n/a
	Diffusivity factors				
Diazepam	3.12	43.6	n/a	—	n/a
Verapamil	2.52	58.8	2.52	84.3	1
Antipyrine	1.13	38.6	n/a	—	n/a

Note: P-gp, P-glycoprotein; CV%, coefficients of variation.
[a] [^{3}H]-verapamil only.

sistent with literature for nasal delivery of small molecules. It has been shown previously that uptake of low-molecular-weight molecules across the olfactory epithelium is dependent on the physicochemical properties of the compound and that CNS uptake by this pathway correlates with lipophilicity (21).

Serial sectioning of the brain revealed that tissue exposure (i.e., AUC in discrete slices) after nasal delivery was dependent on the specific brain region. Regardless of the substrate examined, nasal delivery resulted in preferential exposure in the rostral portions of the brain; exposure decreased consistently as the compound distributed caudally. The profile for [^{3}H]-sucrose supports the premise that the direct olfactory epithelial pathway was being probed. Although [^{3}H]-sucrose appeared in brain after nasal administration, it did not distribute beyond the olfactory region. Furthermore, no [^{3}H]-sucrose was detectable in the brain after systemic administration (Fig. 5). Thus, the amount observed in brain after nasal administration was the result of a direct nose-to-brain transport. The most lipophilic compound tested, [^{14}C]-diazepam, had the highest total exposure, likely due to efficient diffusion through the olfactory epithelium into the brain. The shape of the profiles for nasally administered [^{14}C]-antipyrine and [^{3}H]-verapamil [in the *mdr1a*(–/–) animals] were similar to that for [^{14}C]-diazepam, although these compounds had a somewhat lower total exposure, consistent with a lower lipophilicity.

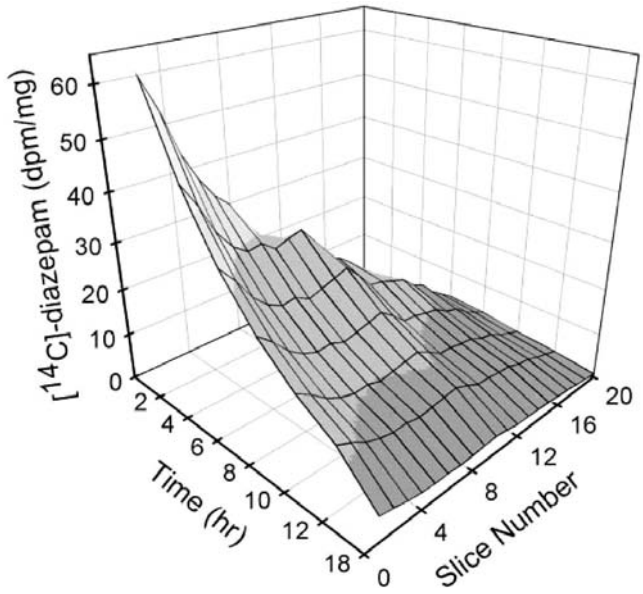

Fig. 7. Three-dimensional representation of the brain disposition of [^{14}C]-diazepam after nasal administration accounting for the influence of time and region on substrate exposure showing the influence of both brain region and time after administration on substrate accumulation.

Compared to nasal administration, systemic administration resulted in a more homogenous distribution of substrate in brain. The total exposure for the compounds was slightly increased (<1.5-fold) compared to nasal administration [43.8 ± 8.9, 35.4 ± 7.8, and 25.9 ± 6.2 %dose*h/mg for [^{14}C]-diazepam, [^{3}H]-verapamil (in *mdr1a*(–/–) mice), and [^{14}C]-

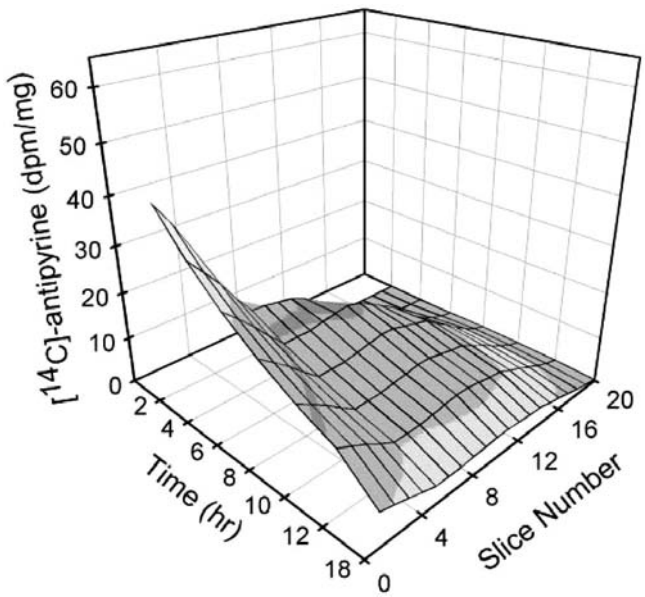

Fig. 8. Three-dimensional representation of the brain disposition of [^{14}C]-antipyrine after nasal administration accounting for the influence of time and region on substrate exposure showing the influence of both brain region and time after administration on substrate accumulation.

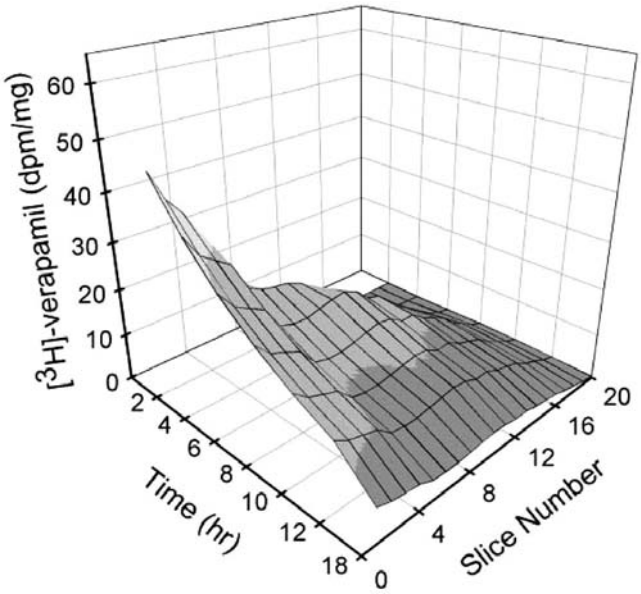

Fig. 9. Three-dimensional representation of the brain disposition of [^{3}H]-verapamil [in *mdr1a*(–/–) mice] after nasal administration accounting for the influence of time and region on substrate exposure showing the influence of both brain region and time after administration on substrate accumulation.

antipyrine, respectively]. Interestingly, substrate persistence in brain appeared to be lower after systemic compared to nasal administration (data not shown), consistent with previous observations that nasal delivery results in increased residence time in the brain (27). In addition, a distinctly lower exposure was noted for all compounds (except sucrose) between slices nos. 7–10. Anatomically, these slices are composed of the parietal cortex, striatum, and thalamus, which are brain regions with relatively low blood volume (25). If

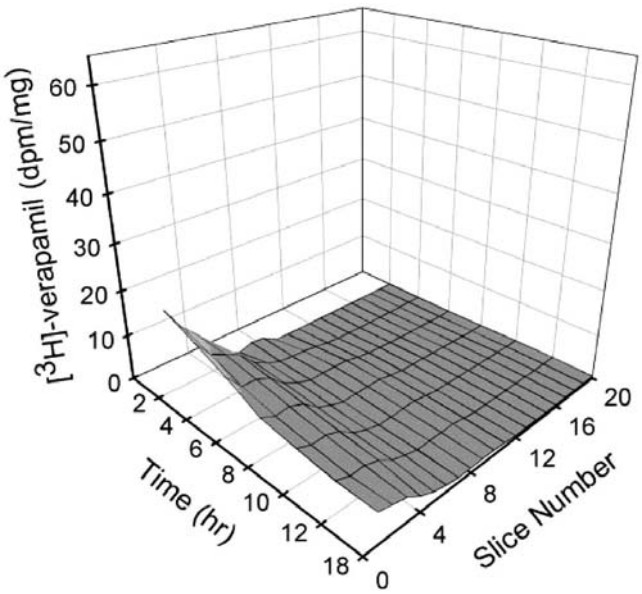

Fig. 10. Three-dimensional representation of the brain disposition of [^{3}H]-verapamil [in *mdr1a* (+/+) mice] after nasal administration accounting for the influence of brain region, time after administration, and P-gp–mediated efflux on substrate exposure.

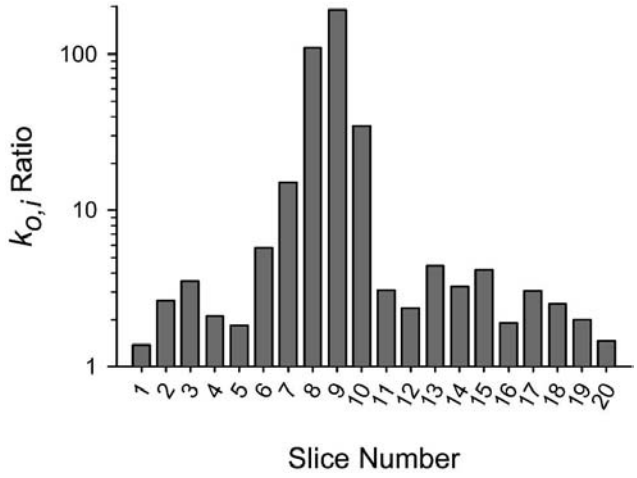

Fig. 11. P-gp effect of [^{3}H]-verapamil loss from individual slices (i = slice number). P-gp effect is expressed as the ratio of k_{oi} estimates in *mdr1a*(+/+) vs. *mdr1a*(–/–) animals. Note that the y-axis is shown as a log scale.

resident blood volumes and blood flow are related, one would anticipate decreased exposure in regions with low blood volume prior to attainment of complete distribution equilibrium. The ability to detect regional differences in substrate exposure that have a known physiologic correlate suggests that the coronal slicing method is sufficiently sensitive to reveal nuances in brain distribution.

The presence of P-gp–mediated efflux resulted in significantly reduced net [^{3}H]-verapamil delivered to the brain (Fig. 2). Also, the profile for [^{3}H]-verapamil distribution in *mdr1a*(+/+) brain compared to *mdr1a*(–/–) animals (Fig. 4) differed somewhat in shape with significantly reduced total exposure, suggesting that P-gp–mediated efflux influenced both initial brain uptake and overall brain distribution after nasal administration.

Because it appeared that serial sectioning was sufficiently sensitive to explore compound distribution within the brain, rigorous mathematical modeling of the data was conducted to further explore and clarify this direct route of delivery. The optimized model (Fig. 1A) was able to describe substrate distribution across time and brain region. Given that [^{3}H]-sucrose failed to distribute significantly past the olfactory region, it was excluded from the modeling exercise. The data from each slice at each time point were modeled simultaneously to generate a comprehensive three-dimensional representation of distribution within the brain as a function of time, distance, and, in the case of [^{3}H]-verapamil, interactions with an efflux transporter (Figs. 7–10). Attempts to consolidate the model by grouping adjacent slices provided inferior results, perhaps due to subtle differences in distribution kinetics between discrete brain regions. The model recovered a single slice-to-slice distributional rate constant for all test compounds, which was modulated by a compound-specific diffusivity factor related to lipophilicity. This result indicates that, in the absence of transporter-mediated flux, physicochemical properties of the compound (i.e., lipophilicity) serve as the primary determinant of brain uptake and distribution.

The results of the modeling for [^{3}H]-verapamil were consistent with earlier work indicating that P-gp is functional at the olfactory epithelium and serves to attenuate brain uptake

after nasal administration (19). These results also clearly show that P-gp operates throughout the brain to efflux substrates during rostral-to-caudal distribution. However, the magnitude of the influence of P-gp on substrate residence in brain evidenced distinct regionality. In contrast to compounds such as diazepam that rely solely on diffusional translocation, the brain distribution of substrates of efflux transporters (in this case, P-gp) is dominated by the transporter-mediated process.

Incorporation of P-gp–mediated efflux into the model led to several interesting quantitative results. P-gp was modeled at the nasal mucosa and the olfactory epithelium (represented by the rate constants k_{np} and k_{1p}, respectively); both sites of expression influenced net uptake of [^{3}H]-verapamil into brain from the nasal cavity. P-gp also was modeled throughout the brain (presumably at the BBB), facilitating loss of substrate from each slice. However, the impact of P-gp on substrate distribution varied significantly among brain regions. The k_{oi} ratio between P-gp–competent and P-gp–deficient animals defined the P-gp effect on substrate persistence in each slice. Between slices nos. 6–10 (anatomically corresponding to the thalamus, striatum, and parietal cortex regions; Fig. 11), the P-gp effect was significantly higher than in other regions of the brain. This regionality in P-gp–mediated flux is consistent with recent literature suggesting preferential P-gp induction in the striatum and frontal cortex in a rat seizure model (28), and may suggest an increased basal expression of P-gp in this region. The significance of this observation is not entirely clear, but the pharmacologic implications are apparent. In order to be an effective CNS agent, a compound must be able to access its pharmacologic target. Opioid receptors are concentrated in the thalamus and cortex (29), and the increased P-gp function in these regions suggests that this may serve a protective mechanism for these and perhaps other key receptors. Further studies are needed to elucidate the significance of the apparent regionality in P-gp function within the brain regions.

Both the data and modeling support the direct pathway of delivery via the olfactory epithelium as the primary route of brain uptake for these compounds. Although the current experiments cannot rule out the contribution of the olfactory nerve pathway, the modeling and time frame of the experiments suggest that the primary pathway of delivery being explored is likely direct. It is possible that the direct pathway and the olfactory nerve pathway work coordinately, although such coordination has not been documented. Alternatively, it is possible that exposure via the systemic circulation contributes to rapid substrate appearance in brain. However, the mathematical modeling did not support the presence of significant drug uptake via this route. In addition, it should be noted that this work examined total radioactivity and therefore might represent the disposition of both parent and one or more derived metabolites.

The fact that millions of people are afflicted with debilitating CNS disorders such as Alzheimer and Parkinson diseases suggests that discovery and development of novel CNS agents will continue at a significant pace. It is imperative that new therapeutic regimens are able to reach relevant pharmacologic target within the brain. Nasal delivery may allow a drug to access a target in the brain more readily than by other routes of administration. However, the mechanisms governing this uptake are only beginning to be understood. In order to exploit this potential delivery route, efforts must be focused on increasing the fraction of the dose that reaches the CNS. A comprehensive characterization of the potential transporters and metabolic enzymes present at the "nose-brain barrier" is required in order to maximize the potential that this delivery route may offer.

ACKNOWLEDGMENTS

Funding for this research was provided by NIH grant GM61191.

REFERENCES

1. C. L. Graff and G. M. Pollack. Drug transport at the blood-brain barrier and the choroid plexus. *Curr. Drug Metab.* **5**:95–108 (2004).
2. R. B. Kim, M. F. Fromm, C. Wandel, B. Leake, A. J. Wood, D. M. Roden, and G. R. Wilkinson. The drug transporter P-glycoprotein limits oral absorption and brain entry of HIV-1 protease inhibitors. *J. Clin. Invest.* **101**:289–294 (1998).
3. W. Loscher and H. Potschka. Role of multidrug transporters in pharmacoresistance to antiepileptic drugs. *J. Pharmacol. Exp. Ther.* **301**:7–14 (2002).
4. E. M. Kemper, A. E. van Zandbergen, C. Cleypool, H. A. Mos, W. Boogerd, J. H. Beijnen, and O. van Tellingen. Increased penetration of paclitaxel into the brain by inhibition of P-glycoprotein. *Clin. Cancer Res.* **9**:2849–2855 (2003).
5. R. L. Juliano and V. Ling. A surface glycoprotein modulating drug permeability in Chinese hamster ovary cell mutants. *Biochim. Biophys. Acta* **455**:152–162 (1976).
6. V. Ling. Multidrug resistance: molecular mechanisms and clinical relevance. *Cancer Chemother. Pharmacol.* **40**:S3–S8 (1997).
7. P. F. Juranka, R. L. Zastawny, and V. Ling. P-glycoprotein: multidrug-resistance and a superfamily of membrane-associated transport proteins. *FASEB J.* **3**:2583–2592 (1989).
8. E. Beaulieu, M. Demeule, L. Ghitescu, and R. Beliveau. P-glycoprotein is strongly expressed in the luminal membranes of the endothelium of blood vessels in the brain. *Biochem. J.* **326**: 539–544 (1997).
9. F. J. Sharom. The P-glycoprotein efflux pump: how does it transport drugs? *J. Membr. Biol.* **160**:161–175 (1997).
10. A. R. Safa. U. S. Rao, S. L. Nuti, T. W. Loo, M. C. Bartlett, and D. M. Clarke. Identification and characterization of the binding sites of P-glycoprotein for multidrug resistance-related drugs and modulators. *Curr. Med. Chem. Anti-Canc. Agents* **4**:1–17 (2004).
11. W. H. Frey II. Bypassing the blood-brain barrier to delivery therapeutic agents to the brain and spinal cord. *Drug Deliv. Tech.* **2**:46–49 (2002).
12. A. A. Hussain, R. Kimura, and C. H. Huang. Nasal absorption of testosterone in rats. *J. Pharm. Sci.* **73**:1300–1301 (1984).
13. J. Henriksson, J. Tallkvist, and H. Tjalve. Uptake of nickel into the brain via olfactory neurons in rats. *Toxicol. Lett.* **91**:153–162 (1997).
14. H. S. Chow, Z. Chen, and G. T. Matsuura. Direct transport of cocaine from the nasal cavity to the brain following intranasal cocaine administration in rats. *J. Pharm. Sci.* **88**:754–758 (1999).
15. A. A. Hussain. Intranasal drug delivery. *Adv. Drug Deliv. Rev.* **29**:39–49 (1998).
16. S. Perlman, E. Barnett, and G. Jacobsen. Mouse hepatitis virus and herpes simplex virus move along different CNS pathways. *Adv. Exp. Med. Biol.* **342**:313–318 (1993).
17. R. G. Thorne, C. R. Emory, T. A. Ala, and W. H. Frey II. Quantitative analysis of the olfactory pathway for drug delivery to the brain. *Brain Res.* **692**:278–282 (1995).
18. H. H. Chow, N. Anavy, and A. Villalobos. Direct nose-brain transport of benzoylecgonine following intranasal administration in rats. *J. Pharm. Sci.* **90**:1729–1735 (2001).
19. C. L. Graff and G. M. Pollack. P-glycoprotein attenuates brain uptake of substrates after nasal instillation. *Pharm. Res.* **20**:1225–1230 (2003).

20. Y. Wang, R. Aun, and F. L. Tse. Brain uptake of dihydroergotamine after intravenous and nasal administration in the rat. *Biopharm. Drug Dispos.* **19**:571–575 (1998).
21. T. Sakane, M. Akizuki, S. Yamashita, T. Nadai, M. Hashida, and H. Sezaki. The transport of a drug to the cerebrospinal fluid directly from the nasal cavity: the relation to the lipophilicity of the drug. *Chem. Pharm. Bull. (Tokyo)* **39**:2456–2458 (1991).
22. L. Illum. Nasal drug delivery–possibilities, problems and solutions. *J. Control. Rel.* **87**:187–198 (2003).
23. P. Arora, S. Sharma, and S. Garg. Permeability issues in nasal drug delivery. *Drug Discov. Today* **7**:967–975 (2002).
24. L. Illum. Transport of drugs from the nasal cavity to the central nervous system. *Eur. J. Pharm. Sci.* **11**:1–18 (2000).
25. C. Dagenais, C. Rousselle, G. M. Pollack, and J. M. Scherrmann. Development of an in situ mouse brain perfusion model and its application to mdr1a P-glycoprotein-deficient mice. *J. Cereb. Blood Flow Metab.* **20**:381–386 (2000).
26. M. A. Wioland, J. Fleury-Feith, P. Corlieu, F. Commo, G. Monceaux, J. Lacau-St-Guily, and J. F. Bernaudin. CFTR, MDR1, and MRP1 immunolocalization in normal human nasal respiratory mucosa. *J. Histochem. Cytochem.* **48**:1215–1222 (2000).
27. W. A. Banks, M. J. During, and M. L. Niehoff. Brain uptake of the glucagon-like Peptide-1 antagonist exendin(9-39) after intranasal administration. *J. Pharmacol. Exp. Ther.* **309**:469–475 (2004).
28. A. Lazarowski, A. J. Ramos, H. Garcia-Rivello, A. Brusco, and E. Girardi. Neuronal and glial expression of the multidrug resistance gene product in an experimental epilepsy model. *Cell. Mol. Neurobiol.* **24**:77–85 (2004).
29. C. E. Inturrisi. Clinical pharmacology of opioids for pain. *Clin. J. Pain* **18**:S3–13 (2002).